HELLENIC REPUBLIC
National and Kapodistrian University of Athens

School of Science

Department of Geology and Geoenvironment

Investigation of REE-fluorcarbonate Minerals

BSc Thesis

ORESTIS DIMOPOULOS

Supervisor: Prof. A. Godelitsas

Athens, 2023

Acknowledgements

Prof. S. Xanthos (International Hellenic University) is thankfully acknowledged for his exceptional expertise and assistance in γ-ray spectroscopy measurements. Also, Prof. S. Karavoltsos (N&K University of Athens / UoA) for his assistance with ICP-MS measurements. Finally, Dr. A. Papoutsa (UoA) for her contribution in Raman spectroscopy.

Abstract

This study focuses on the investigation of REE fluorcarbonate-minerals, with special emphasis to actinide elements (mainly Th, U). The samples studied included parisite and bastnäsite crystals, as well as a typical REE-containing rock (carbonatite). Optical microscopy, XRD, and SEM-EDS, were utilized to characterize the aforementioned geological materials. The actinide elements (particularly Th in high concentration) were detected in point analyses by SEM-EDS. A complementary ICP-MS bulk analysis was performed for U in the case of the parisite crystals, which revealed a content of 64 ppm, in accordance to previous literature. Laser micro-Raman Spectroscopy was used to identify μm-sized inclusions, proved to be goethite. Measurements by γ-ray Spectroscopy further quantified high radioactivity due to Th-232 (57,726 Bq/kg), as well as considerable one due to U-238 (599 Bq/kg). These findings enhance our understanding of actinide mineralogy & geochemistry in REE fluorcarbonate minerals, and demonstrate the need for more relevant research in respect of REE raw materials and resources.

1. INTRODUCTION

1.1 Rare Earth Elements

Rare Earth Elements (REE) concern seventeen elements of the Periodic Table, namely the lanthanides, together -occasionally- with yttrium (Y) and scandium (Sc). This name was given to them in the 18th Century, due to the fact that when they were discovered they were considered rare. Nowadays it is a known fact that REEs are not rare at all, as some of them are as abundant as copper (Cu). However, they don't typically occur at high enough concentrations to be easily mined.

Nowadays, REEs are part of a wider group of elements called "critical metals". These metals are indispensable to emerging technologies and to the energy sector. From their use in batteries of electric cars to their application in permanent magnets on wind turbines, critical metals and REE in particular play an irreplaceable role in new technological innovations that help shift society to the use of cleaner energy. However, the applications of REEs don't stop there. They are used as components in high technology devices such as cell phones, computer monitors, catalytic converters, etc. and are also heavily used in the defense sector since many night-vision goggles, GPS equipment, precision-guided weapons etc. are manufactured using rare earth metals as their key elements. Given their wide applications in different sectors of everyday life and their importance in future technologies, it isn't surprising why the research for REEs has soared the past years and why REEs deposits are sought after globally.

1.2 REE-fluorcarbonate minerals & deposits

Rare earth elements (REEs) are highly coveted due to their crucial role in a wide array of technological applications. However, their occurrence in nature is primarily in trace amounts, rendering conventional mining methods economically impractical for their extraction. Consequently, the industry seeking to exploit and mine REEs focus its efforts on identifying minerals with high concentrations of these elements. A group of minerals known as

fluorcarbonate minerals have garnered significant attention in this regard. These minerals derive their name from their chemical composition, which incorporates fluoride (F^-) and carbonate ions (CO_3^{2-}) into their structure (e.g. Grice at al. 2007). Fluorcarbonate minerals are typically rare. The most known fluorcarbonate mineral is bastnäsite [$(REE)CO_3F$]. Bastnäsite and another fluorcarbonate mineral called synchysite [$Ca(REE)(CO_3)_2F$] form a mineral series in which these two minerals, with cerium (Ce) as their dominant REE, present its end members. Relevant minerals that are acknowledged are those of the parisite [$CaCe(CO_3)_3F_2$] group and röntgenite [$CaCe(CO_3)_5F_3$] (e.g. Christy et al. 2021). In this series, the minerals present many similarities with each other in their physical properties and usually analytical methods are required in order to distinguish each mineral phase. It must be noted that fluorcarbonate minerals are typically sources of Light REE (LREE), meaning from Lanthanum (La) to Gadolinium (Gd), whereas Heavy REE (HREE), which are the elements from Terbium (Tb) to Lutetium (Lu), are usually found in phosphate phases like xenotime [$(Y,HREE)PO_4$] and in minerals that are a part of the apatite group.

Fluorcarbonate minerals are primarily found in alkali igneous rocks called carbonatites. These rocks contain over 50% wt. carbonate minerals such as calcite, dolomite, ankerite, etc. Carbonatites have been present in over 600 places around the world, mainly in continental areas but in multifarious tectonic settings (**Fig. 1**). The high variability of carbonatites' occurrences has raised many questions and controversies concerning the processes that resulted in their formation. This wide range of processes includes fractional crystallization, liquid immiscibility, post-magmatic alteration, and melt generation. Currently, there are three main hypotheses for the genesis of carbonatites (**Fig. 2**).

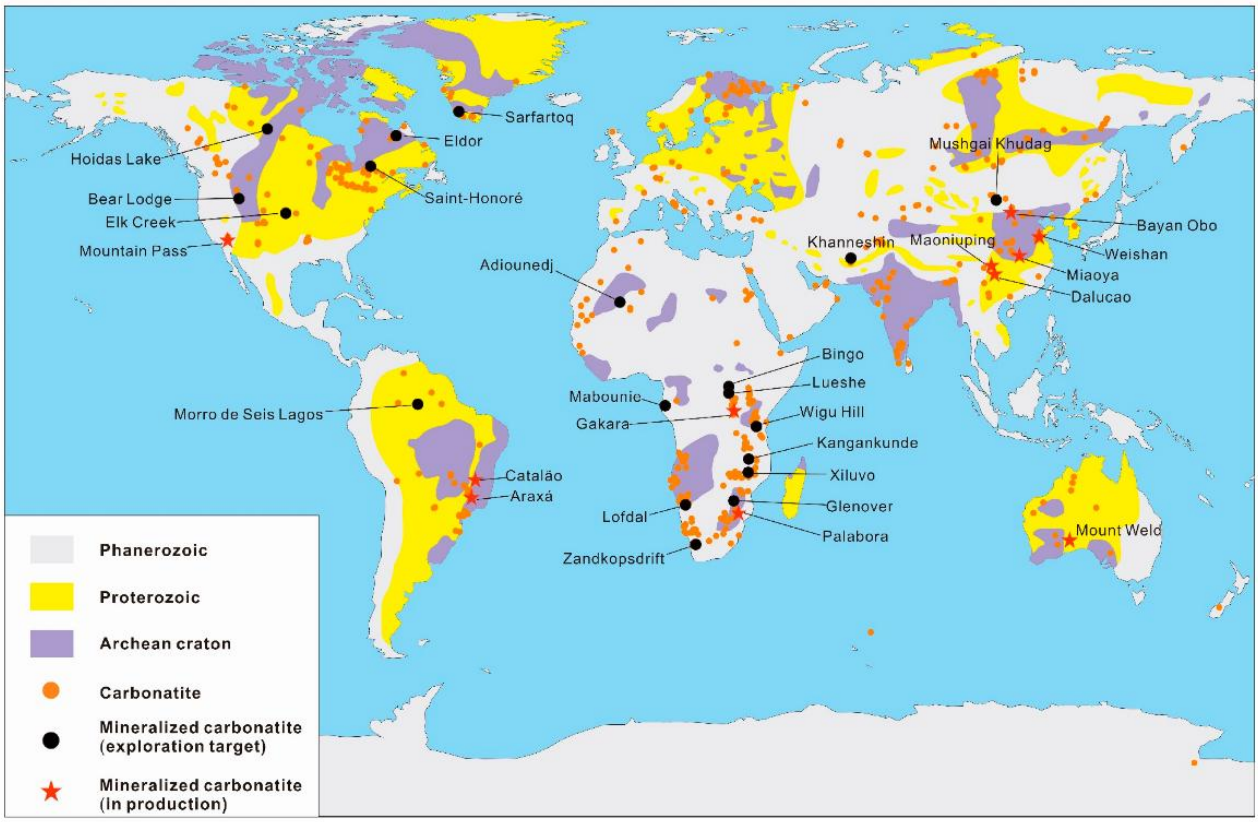

***Figure 1**: Global carbonatites distribution (https://www.mdpi.com/2075-163X/10/11/965)*

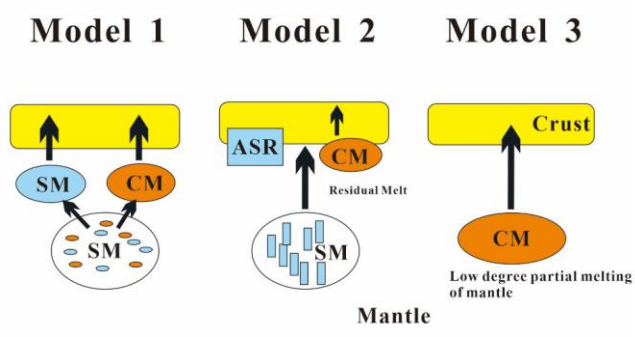

***Figure 2**: Three main models explaining the genesis of carbonatites. (Model 1) Segregation due to immiscibility of a carbonate magma from a silicate magma. (Model 2) Fractional crystallization of a Si-undersaturated carbonatitic melt. (Model 3) low degree partial melting of the mantle; CM—carbonate melts; SM—silicate melts; ASR—alkaline silicate rocks (https://www.mdpi.com/2075-163X/10/11/965)*

One hypothesis proposes that an alkali-rich carbonatite magma was generated by partial melting of a CO_2-bearing mantle peridotite or eclogite at a pressure exceeding 2 GPa. This magma, due to lithostatic stress, may have ascended and reacted with surrounding pyroxenites, forming wehrlite. The wehrlite could have acted as a shield for the carbonatitic melt as it reached the crust, or the melt may have ascended directly via fractures. High levels of nickel (Ni) and chromium (Cr) would need to be detected to support this hypothesis. The second hypothesis is that of fractional crystallization. According to this hypothesis, a silica-undersaturated carbonate melt suffered fractional crystallization and the residual high in alkalis melt evolved into a carbonatitic liquid without intersecting a two-liquid solvus. This means that the temperature-pressure conditions were such that immiscibility didn't occur (e.g. Yaxley et al. 2021). The last hypothesis concerning the formation of carbonatites proposes that carbonatites occurred from an immiscible carbonate magma that segregated from CO_2-bearing, silica-undersaturated, silicate magma. Due to fractional crystallization of a peridotite containing a few 1,000 ppm C, in high pressures and low melt fractions, a SiO_2-undersaturated silicate melt can be formed. If this resulting melt separates, then reaches the crust and finally suffers fractional crystallization, the residual silicate liquid will have increased levels of CO_2 and as a result a carbonate liquid may be produced (e.g. Yaxley et al., 2021). Consequently, a carbonatitic magma can be formed. The requirement for this hypothesis is that fractionation of the parental liquid must drive the liquid's composition to the two-liquid solvus that segregates the carbonate and silicate melts. After their formation and emplacement into the crust, carbonatites are subject to secondary evolutionary processes. Interactions with meteoric water and hydrothermal fluids cause chemical alterations within the carbonatites. These interactions happen at a post-magmatic stage in the evolutionary process of a carbonatite, and they can be responsible for the concentration of REEs (e.g. Yaxley et al., 2021). One frequent process that results in the concentration of REEs is called "fenitization". Fenitization is a metasomatic process that occurs when the carbonatitic melt exsolves an alkali-rich fluid that infiltrates into the surrounding country rock and causes metasomatism. As a result, alkali-rich silicate gangue minerals can appear, such as alkali feldspars (e.g albite, sanidine) and inosilicates (pyroxenes and amphiboles) (e.g. Yaxley et al., 2021).

The chemical composition of REE mineralizing fluids is key to the understanding of the formation of REE ore deposits in carbonatites. As REEs are incompatible elements,

crystallization of REE-rich minerals occurs in the later stages of crystal fractionation in lower temperatures than their respective REE-poor and Fe-, Mg- rich minerals that form at first, such as olivine, magnetite and clinopyroxene (e.g. Anenburg et al., 2021). The residual melt, rich in alkalis, fluoride, chloride, sulfate and REEs, forms a brine-melt at ~ 400 ^{o}C. The REEs that are concentrated in the brine-melt may form alkali REE carbonates that are very ephemeral like burbankite [$(Na,Ca)_3(Sr,Ba,Ce)_3(CO_3)_5$] and carbocernaite [$(Ca,Na)(Sr,Ce,Ba)(CO_3)_2$], monazite [$REE(PO_4)$] and in some cases fluoroapatite [$Ca_5(PO_4)_3F$] which can contain substantial amounts of LREEs. However, the concentration of REEs in these fluorcarbonate minerals isn't enough to justify the formation of REE ore deposits in carbonatites. That is why it has been proposed that in later post-magmatic stages, hydrothermal fluids cause recrystallization of these fluorocarbonate minerals, into less soluble, calcic minerals such as bastnäsite, parisite, etc. (e.g. Anenburg et al., 2021). It has been suggested that the hydrothermal fluids responsible for the aforementioned recrystallization carry REEs as chloride and sulfate complexes whereas fluoride and carbonate serve as precipitating ligands. This model however doesn't agree with all field observations, mainly in localities where fenite aureoles around carbonatitic intrusions indicate the circulation of "basic" in nature hydrothermal fluids, compared to the more "acidic" complexes that are mentioned above. In answer of this conundrum, recent studies (e.g. Anenburg et al.,2021; Louvel et al., 2022) have shown that carbonate- and alkali-rich fluids can carry large amounts of REEs along with fluoride. Under acidic conditions, fluoride in hydrothermal fluids serves as the depositional ligand to the REEs and isn't involved in their mobilization. However, carbonate- and alkali-rich fluids have shown to be able to efficiently transport LREEs even with the addition of fluoride in their composition, thus depositing LREE-bearing fluorcarbonate minerals under the right conditions (e.g. Louvel et al., 2022).

1.3 Actinides in REE-fluorcarbonate minerals and carbonatites

In carbonatites, aside from the lanthanides, that are of economic and technological importance, also occur actinides, mainly uranium (U) and thorium (Th). These are two radioactive elements just like all other actinides, that have many applications. Uranium is predominantly used as fuel for nuclear reactors and certain isotopes of U have uses in the medical, industrial and defense sectors. Thorium on the other hand, which is a much more abundant element in nature than

uranium but less radioactive, even though it is a radioactive element as well, it hasn't been used as fuel for nuclear reactors yet because of its fertile and not fissile properties. However, it is widely used as an industrial catalyst and in the aerospace industry, among other sectors.

The radioactivity recorded in all carbonatitic bodies originate from these actinides which can be mined as by-products of REE mining. Not every REE deposit is also a source of Th and U but they all have elevated concentration of these elements. Even though there are plenty of U and Th primary ore minerals, in carbonatites U and Th are mainly found in their tetravalent states inside the structure of different oxides such as perovskite [$CaTiO_3$], zirconolite [$CaZrTi_2O_7$], and pyrochlore [$(Na,Ca)Nb_2O_6F$] group minerals, where they substitute for Ca^{2+}, Na^{+} and less often Zr^{4+} (e.g. Kogarko et al, 2013). The main hosting phases of actinides in carbonatites are the pyrochlore group minerals which are usually paragenetically enriched in U and Th during their early crystallization stage. For Th in particular, excluding the presence of its primary ore mineral thorianite [ThO_2] in some carbonatitic bodies, it is predominantly extracted as a by-product from the mining of a REE-phosphate mineral monazite [$(Ce,La,Nd,Th)PO_4$].

1.4 Previous work and scope of the present study

To the best of our knowledge, even though there is an extensive literature regarding fluorcarbonate minerals and their relationship with REEs, there hasn't been any previous work that emphasizes on the presence of actinides (U, Th) in these geological materials. However, it must be noted that, in many studies concerning fluorcarbonate mineral deposits, the U and Th contents are sometimes reported but not radioactivity accurate measurements.

Within the frame of the present study, the fluorcarbonate mineral samples originated in Snowbird deposit in Montana/USA (parisite) and the Andakatany deposit in Madagascar (bastnäsite). A typical relevant rock (carbonatite) from the Buru Hill deposit in Kenya was also examined. For the fluorcarbonate mineral crystals that have been investigated in this work, previous authors have provided with some evidence for the presence of actinide elements (mainly U, Th). Specifically, for the mineral parasite-(Ce) that is found in Snowbird deposit in Montana/USA, it has been reported an unusually high Th content (up to 17,200 ppm) and less

amount of U (53-57.4 ppm), all aged at 71.1 ± 1 Ma ago (e.g. Metz et al., 1985; Samson et al. 2004). In the Andakatany deposit in Madagascar, it has been reported (e.g. Rasoamalala et al., 2014) that the orthogneiss, which constitutes the host rock of the deposit, contains 12 ppm Th and 3 ppm U. However, there is no literature indicating that the bastnäsite crystals in the Andakatany deposit have been investigated regarding their content in U and Th. Moreover, Onuonga (1997) and Onuonga and Bowden (2000) extensively studied Buru carbonatites and performed a series of essays in order to identify the mineralogy and geochemistry of these rocks. In this locality, the main REE bearing minerals were fluorcarbonates and phosphates (monazite). The ThO_2 wt.% content in bastnasite in Buru Hill carbonatites varied in different depths. Especially, it was found that the sample from 23 m depth had a ThO_2 content of 4.94 wt.%, which has significant difference from the depths of 35 m and 101 m which had ThO_2 contents of 0.37 wt.% and 0.43 wt.% respectively. Interestingly, parisite was identified at 130 m, which possessed 6.42 wt.% of ThO_2 and synchysite at 197 m with a Th content 0.19 wt.%.

Therefore, the scope of the present work was to characterize REE-fluorcarbonate minerals from the localities described above, and investigate the presence of potential actinide elements (mainly U, Th) by analyses and radioactivity -by γ-ray Spectroscopy- measurements.

2. MATERIALS AND METHODS

2.1 Samples

The REE-fluorcarbonate mineral specimens used for this study (obtained from the personal collection of Prof. A. Godelitsas) were the following:

- **Parisite** crystals from the Snowbird deposit in Montana/USA (**Fig. 3**).
- **Bastnäsite** sample from the Andakatany deposit in Madagascar (**Fig. 4**).

A typical relevant rock (**carbonatite**) from the Buru Hill deposit in Kenya, in the form of thin-polished sections, was also examined (**Fig. 5**).

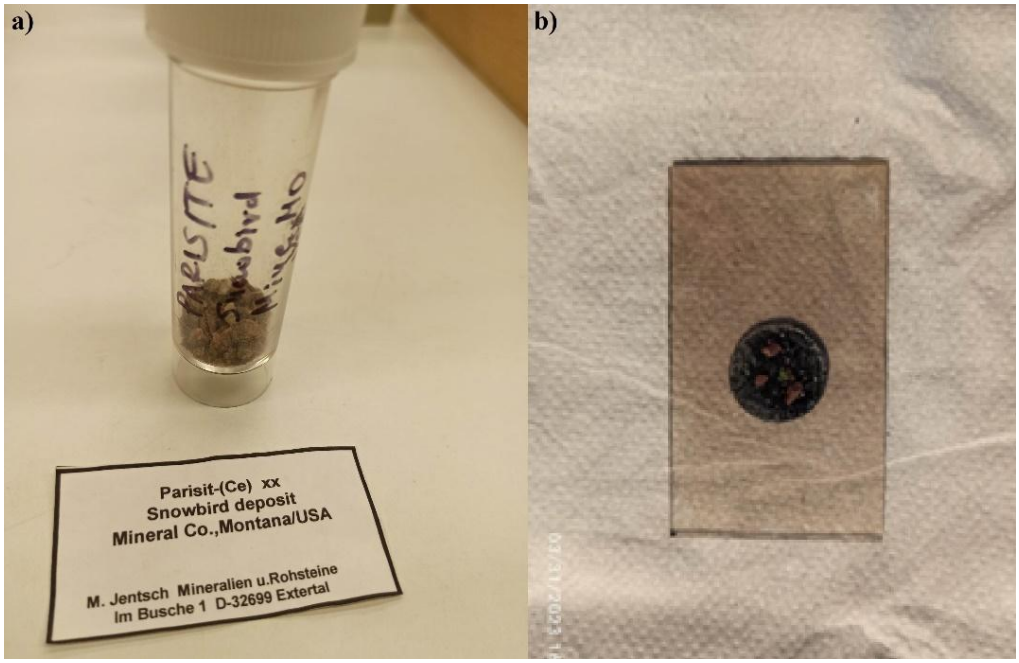

***Figure 3**: a) Parisite crystals from Snowbird deposit, Montana/USA. b) Parisite crystals mounted on C-tape for SEM-EDS investigation*

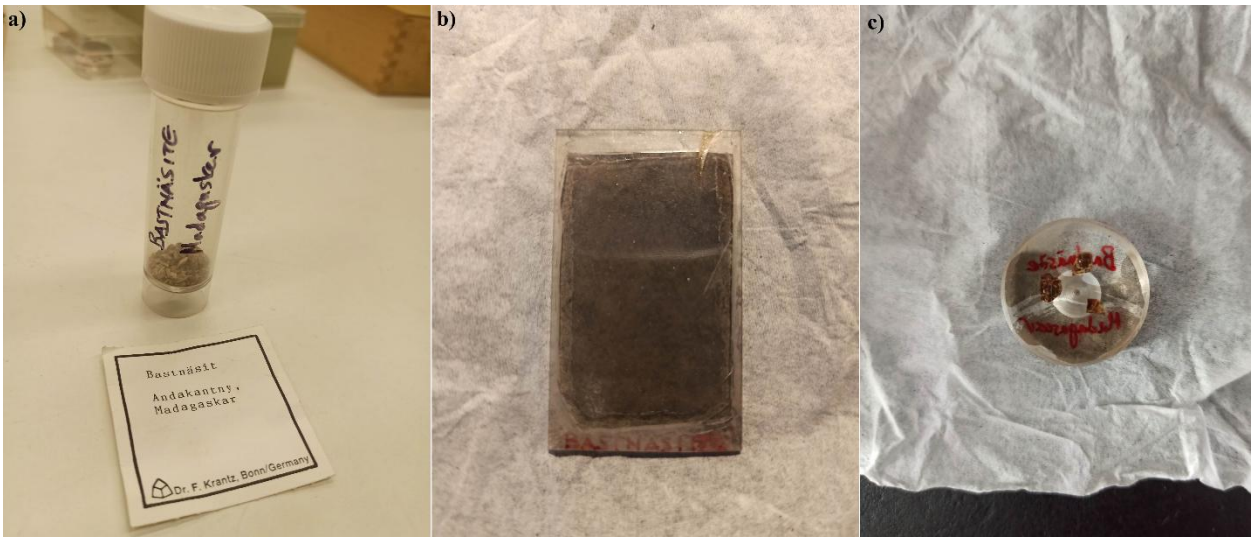

***Figure 4**: a) Bastnäsite crystals from the Andakatany deposit, Madagascar. b) Bastnäsite thin-polished section. c) Bastnäsite polished section.*

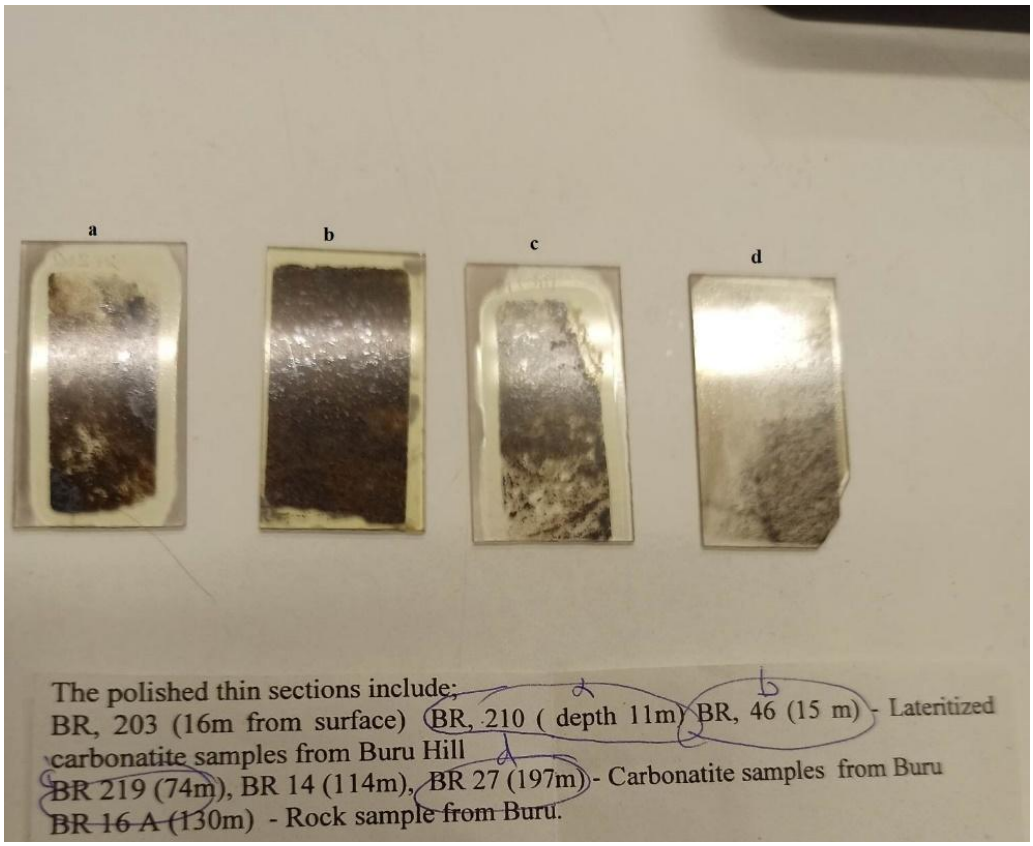

***Figure 5**: Thin-polished sections of a carbonatite from Buru in Kenya. The samples were collected (Onuonga, 1997) from the following depths: a) 11m. b) 15m. c) 74m. d) 197m.*

2.1 Optical Microscopy

The optical microscope (transmitted & reflected light) used in this study was a ZEISS Primotech D/POL model, which offers various technical characteristics for precise observation. The microscope was equipped with a range of objectives, including A-Plan POL lenses with magnifications of 2.5x, 5x, 10x, 20x, and 63x, specifically designed for transmitted illumination. To facilitate imaging and documentation, the microscope was fitted with a tube housing an integrated 3-megapixel CMOS camera, ensuring high-resolution capture of the observed samples.

2.2 Powder X-Ray Diffraction (XRD)

Powder-XRD patterns for all samples were obtained using a Siemens (currently Bruker AXS) D-5005 X-ray diffractometer (CuK_α radiation at 40 kV and 40 mA) and the EVA 10.0 program of the Bruker DIFFRAC plus software package.

2.3 SEM-EDS

The Scanning Electron Microscopic study (SEM-EDS) was performed using a Jeol JSM-5600 SEM equipped with an Oxford EDS, on both free surfaces of the REE-fluorcarbonate minerals and polished sections.

2.4 Chemical analyses for U (ICP-MS)

Bulk chemical analyses, with respect to U, by Inductively Coupled Plasma Mass Spectroscopy, after acid-dissolution of the mineral crystals, were performed using a THERMO ICAP-Qc ICP-MS (**Fig. 6**) and relevant reference materials & solutions. In particular, the initial parisite crystal sample had a total weight of 4.2 g. A portion of 160 mg of powdered sample was dissolved in acid (HNO_3) solution. The mixture was allowed to react for approximately 40 minutes before it was deemed suitable for analysis using ICP-MS. A distinct μm-sized insoluble phase, that was included into the parisite crystal, was kept for further Laser micro-Raman investigation.

***Figure 6**: Thermo ICAP-Qc ICP-MS used for bulk chemical analysis of U .*

2.5 Radioactivity measurements (γ-ray Spectroscopy)

Radioactivity measurements (by γ-ray Spectrsocopy) were performed in the case of selected pure parisite crystals from the Snowbird deposit in Montana/USA. The system included an ultrapure germanium detector from Canberra, namely the BE2020 of the Broad Energy Germanium Detectors series (**Fig. 7**). The simulation of the detector was carried out with a set of Monte Carlo simulations. The mass of the parisite sample that was used for this method was 3.96 10^{-3} kg, with a volume of 1.6619 mL and a density of 2.38281 kg/L.

***Figure 7**: The γ-ray Spectroscopy system used in radioactivity measurements.*

2.6 Laser micro-Raman investigation

The Laser micro-Raman investigation concerned a distinct insoluble phase included into the parisite crystals and performed using a fully-equipped Renishaw system.

3. RESULTS AND DISCUSSION

3.1 Phase identification (optical microscopy, XRD, SEM-EDS)

In the optical microscopy study of the bastnäsite sample from Madagascar, several other mineral phases were identified. The predominant mineral phases observed in the thin-polished sectionw were carbonate minerals; however, precise identification between bastnäsite, calcite, or other

carbonate minerals was challenging based on optical microscopy alone. The presence of quartz, apatite, and feldspars in the sample is consistent with findings reported in the existing literature (Rasoamala et al, 2014). Further observations, in reflected light using polished sections, revealed also the presence of -metallic- Fe-oxides (**Fig. 8 & Fig. 9**).

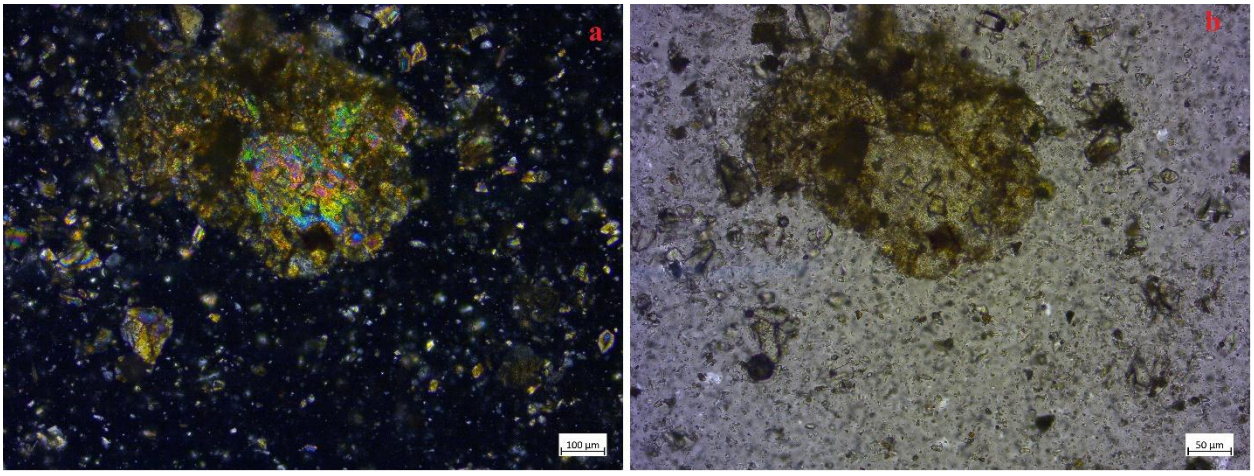

***Figure 8**: Thin-polished section of the bastnäsite sample where carbonate mineral phases and Fe-oxides are observed in transmitted light. (a) X Nicols, (b) // Nicols*

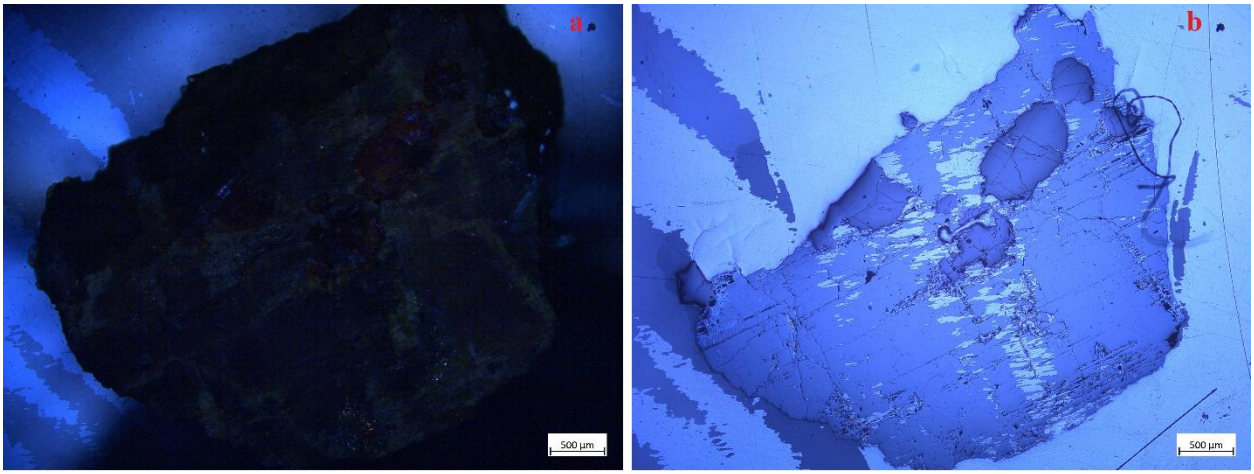

***Figure 9**: Polished section of the bastnäsite sample under reflected light (a) X Nicols, (b) // Nicols*

The REE-bearing rock (carbonatite) samples, obtained from depths of 11, 15, 74, and 197 meters in the Buru Hill deposit in Kenya, exhibit a highly lateritized nature as evidenced by the presence of anhedral and subhedral textures. In all four samples, the primary mineral phases identified were carbonate minerals, accompanied by the occurrence of crystalline and/or amorphous Fe-oxides/oxyhydroxides formed due to the process of lateritization (**Fig. 10**).

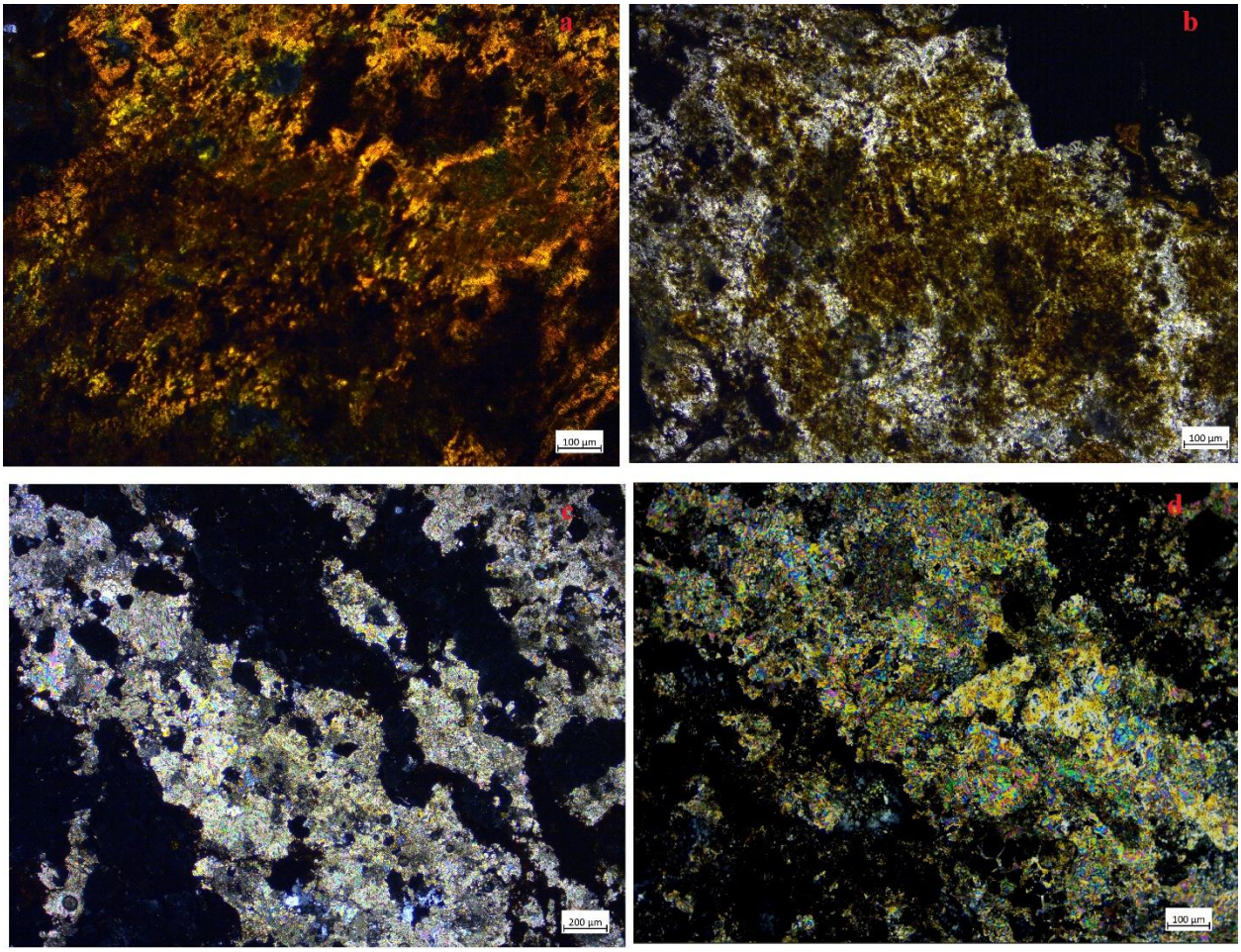

***Figure 10**: Lateritized carbonatite on X Nicols.*

However, using optical microscopy alone, the specific identification of REE-bearing minerals was challenging, indicating that the carbonate mineral phases identified may not correspond to

REE fluorocarbonate minerals such as bastnäsite or parisite. Instead, it suggests the possibility of these REE-bearing fluorocarbonates occurring at a smaller scale. The identified Fe-oxides are likely goethite [FeOOH], hematite [Fe_2O_3], and magnetite [Fe_3O_4]. Regarding REE-bearing minerals, synchysite and parisite are anticipated, with parisite being more stable at depths below 150 meters (Onuonga, 1997; Onuonga and Bowden, 2000). Accessory minerals in this carbonatite sample from Buru Hill in Kenya, as described in the literature, include biotite, apatite, aegirine, and monazite. Fluorite, psilomelane, are also reported among the mineral phases discovered within the carbonatite. However, using optical microscopy alone, these minerals could not be definitively identified in the samples. It is noteworthy that the 11-meter depth sample of the carbonatite displays a pronounced and advanced stage of lateritization, characterized by prominent features indicative of intense alteration processes. These features include the presence of well-developed anhedral and subhedral textures, as mentioned earlier, suggesting a substantial degree of weathering and chemical transformation. As the depth of the samples increases to 15, 74, and 197 meters, the manifestations of lateritization progressively diminish, indicating a decrease in the intensity of weathering and alteration phenomena. This observation implies a spatial variation in the degree of lateritization within the carbonatite, with the shallower sections experiencing a more pronounced and advanced stage compared to the deeper portions.

Concerning the powder-XRD investigation of the REE-fluorcarbonate minerals, a characteristic pattern is shown in **Fig. 11.** This research typically approves the aforementioned minerals.

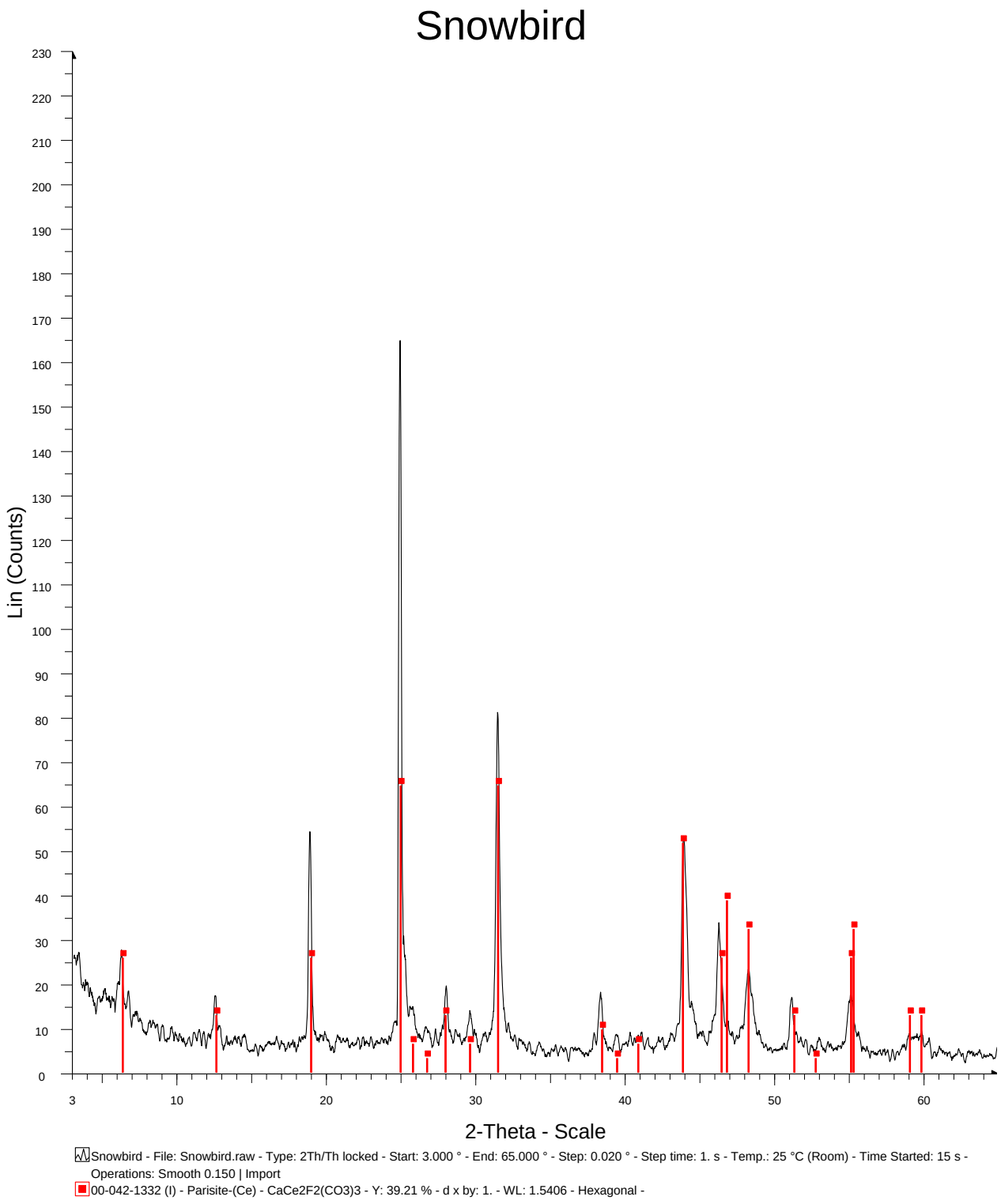

***Figure 11**: Powder-XRD pattern of the Snowbird (Montana, USA) parisite crystals*

The SEM-EDS study conducted on the bastnäsite sample from Madagascar revealed several peaks within the range of 4 keV to 7 keV, which correspond to the *L* X-ray emission lines of lanthanides (REE). This observation confirms the dominant presence of elements such as La, Nd, and Ce in the sample, further supporting the identification of the sample as bastnasite. Given that bastnasite is known to contain mainly light rare earth elements (LREE), the detection of these specific lanthanides was expected (**Fig. 12**).

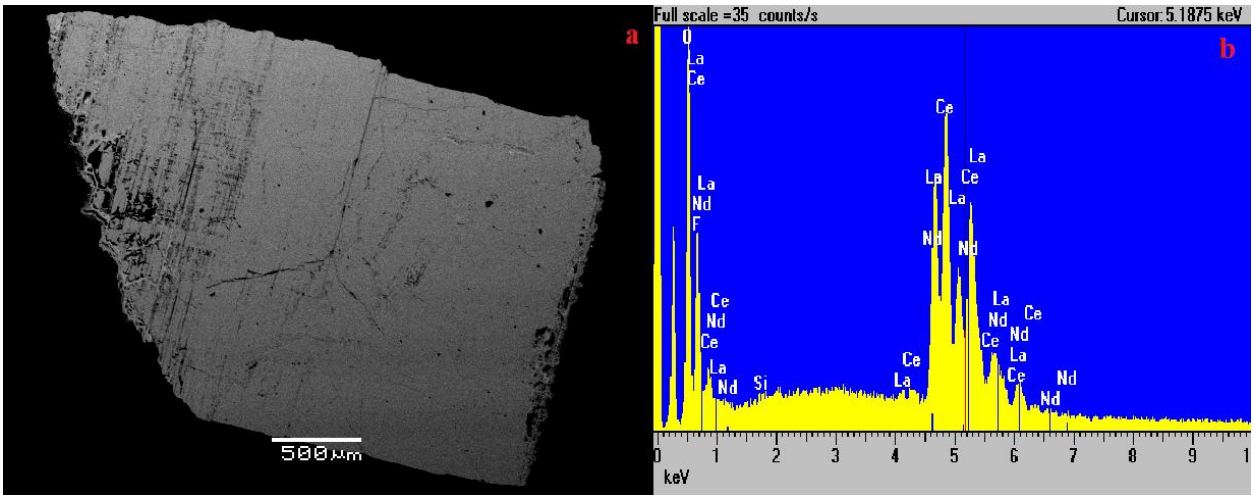

***Figure 12**: a) BSE image of a bastnäsite crystal, b) EDS spectrum of the (a) bastnäsite crystal.*

The point analyses by SEM-EDS also revealed peaks of Al and Si, which means that the sample must contain aluminosilicate inclusions (**Fig. 13**). The bastnäsite in the Andakatany deposit in Madagascar, from which the sample was collected, is hosted in granitic dykes, and it was formed by late-stage hydrothermal processes (Rasoamalala et al., 2013). Therefore, the host rock or the hydrothermal fluids are the most likely sources of Al and Si that were detected in the X-ray spectra of the material.

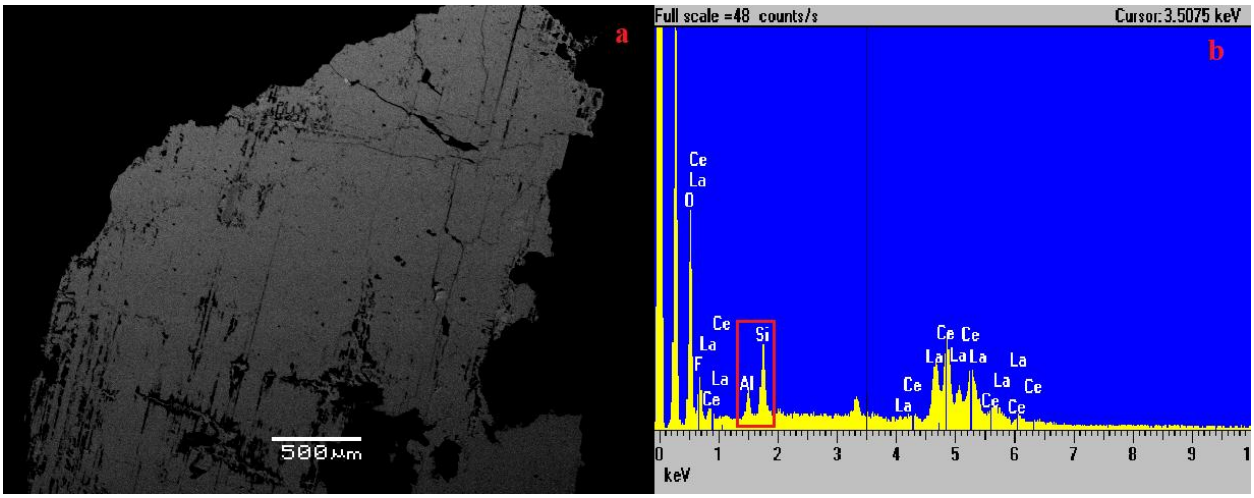

***Figure 13**: a) BSE image of a bastnasite crystal, b) EDS spectrum of the (a) bastnasite crystal. The red highlighted rectangle showcases the Al, Si peaks.*

Similarly, the SEM-EDS investigation of parisite crystals from the Snowbird (Montana, USA) deposit also yielded peaks of Ce, La, and Nd within the expected energy range (**Fig. 14**). In addition, the point analyses in microscale revealed the presence of thorium (Th) in the sample. This finding agrees with a previous study (Metz et al., 1985) that had reported high levels of Th in this deposit. However, the presence of U was not confirmed by SEM-EDS and that led to the necessity to perform separate ICP-MS analyses; see text below. Besides, the high radioactivity of these parisite crystals, due to Th, was finally approved by γ-ray Spectroscopy; see also text below.

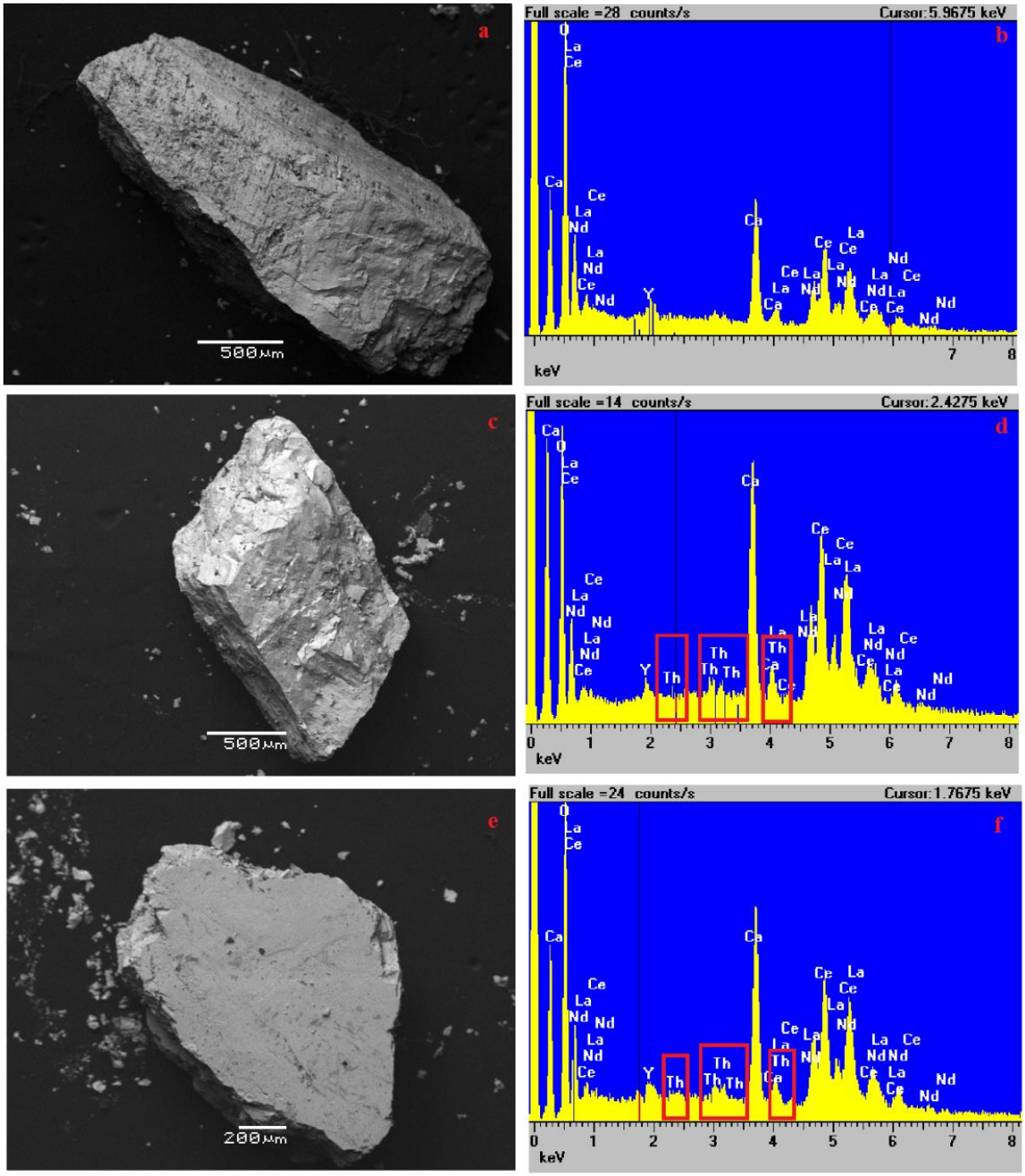

***Figure 14**: a), c), e): BSE images of parisite crystals, b), d), f): EDS spectra of the crystals on the left. The red highlighted rectangles showcase the Th peaks.*

3.2 Parisite actinide (U) content by ICP-MS

The bulk ICP-MS analyses of the pure parisite crystals revealed a U content of 64 ppm. It is evident that this U concentration, although considerable, is generally below the detection limit of the previously used SEM-EDS. The U concentration measured in the present study is in general agreement with the findings of Metz et al. (1985), who reported a range of 54-57 ppm for this fluorcarbonate-mineral from Snowbird deposit in Montana/USA. Besides, it should be noted that the bastnäsite sample from Madagascar was not able to be accurately analyzed for U (or Th) using ICP-MS method due to the presence of many inclusions, as evidenced during the SEM-EDS investigation.

3.3 Laser micro-Raman Spectroscopy of insoluble inclusion in parisite crystals

It must be noted that after the acid-dissolutio of the parisite crystals, distinct μm-sized grain of an unknown mineral phase remained. According to Laser micro-Raman Spectroscopy (**Fig. 15**), the mineral phase was found to be goethite [$Fe^{+3}O(OH)$] with an accuracy of its spectra compared to the spectra of the unknown mineral phase of 83%. This finding means that U analyses by ICP-MS -and also the γ-ray Spectroscopy results- are not affected by the presence of this inclusion, inasmuch it can hardly accommodate considerable quantities of actinides.

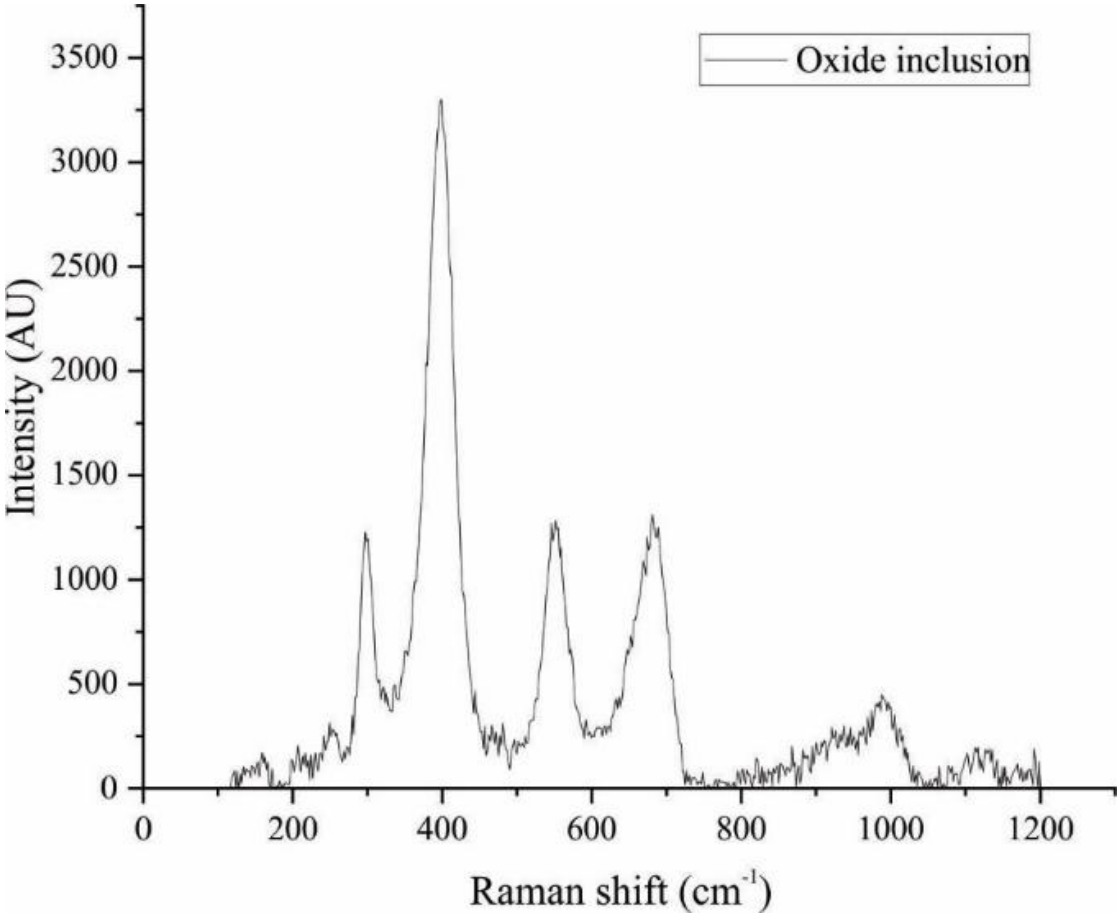

***Figure 15**: Laser micro-Raman spectrum of insoluble μm-sized inclusion into parisite crystals*

3.4 Gamma-ray spectroscopy and radioactivity

The γ-ray Spectroscopy results, indicating enhanced radioactivity of parisite crystals, are presented in **Figs. 16 & 17** and shown in **Table 1**. The radioactivity due to U-238 was calculated to be 699 Bq/kg, utilizing the average value derived from the isotopes Pb-214 and Bi-214. Similarly, the radioactivity due to Th-232 was assessed by analyzing isotopes from the Th-series, namely Ac-228, Pb-212, Bi-212, and Tl-208. The calculated radioactivity due to Th-232 was found to be a substantial, namely 57,726 Bq/kg. These results shed light on the notable presence

of Th in the sample, confirming earlier findings from the literature (Metz et al., 1985). Besides, the γ-ray Spectroscopy results are in line with the bulk ICP-MS measurements with regard to the considerable presence of U in the material. Moreover, the natural radioactivity due to K-40, was measured at 4204 Bq/kg. All the above suggest that Th is the predominant actinide element in the studied parisite crystals, related to substantially higher radioactivity compared to that due to U.

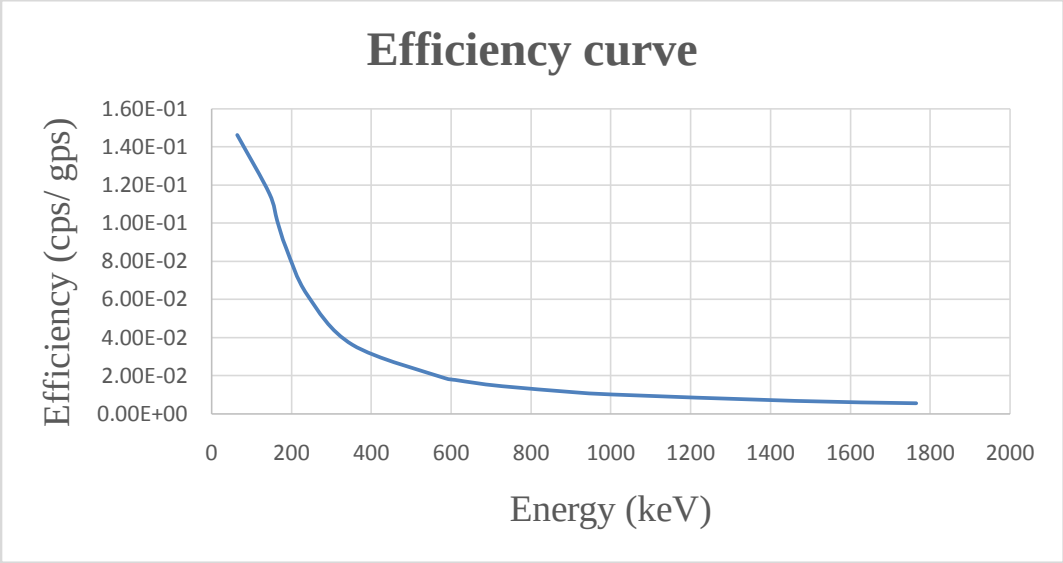

***Figure 16**: Efficiency curve using a set of Monte Carlo simulations.*

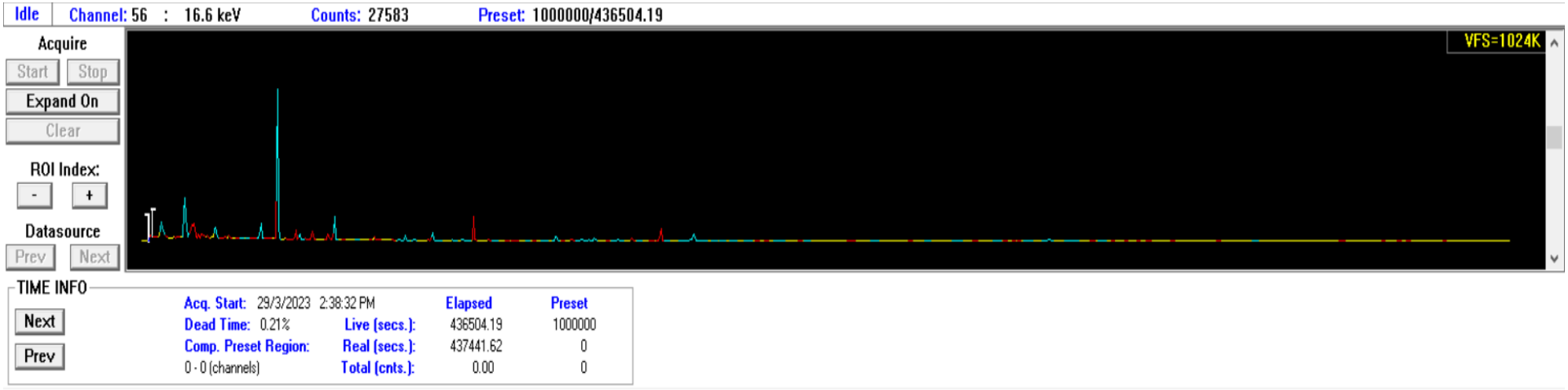

***Figure 17**: Gamma-ray spectrum of parisite crystals.*

Nuclide	Energy	Area	±	Area Interference Correction	Cps	background dec21v2	±	BG/s	Net c/s	±	Efficiency, 260 ml,	efficiency ±	FY	Branching Correction	Bq/Kg	±	MDA
Th-234	**63.5**	0	0	0	0	487	112.01	0.00061685	-0.000617	0.0001419	**0.146368**	**0.0146368**	0.039	0	**-27**	**3**	**0.50**
Pa-234	**1001**	810.38	80.03		0.00185652	87	49.59	0.0001102	0.0017463	0.0001938	**0.0102421**	**0.00102421**	0.01021	0	**4217**	**422**	**7.00**
Ra-226 Gilmore corection	**186.2**	5929.04	315.57	3385.48184	0.0077559	1372	150.92	0.00173781	0.0060181	0.0007478	**0.0870089**	**0.00870089**	0.03533	0	**494**	**49**	**0.80**
Ra-226 ftom 143 keV	**186.2**	5929.04	315.57	6044.14129	0.0138467	1372	150.92	0.00173781	0.0121089	0.0007478	**0.0870089**	**0.00870089**	0.03533	0	**995**	**99**	
Ra-226 from Th-234	**186.2**	5929.04	315.57	6038.228024	0.01383316	1372	150.92	0.00173781	0.0120953	0.0007478	**0.0870089**	**0.00870089**	0.03533	0	**994**	**99**	
Ra-226 from Pa-234	**186.2**	5929.04	315.57	-10945.05171	-0.02507434	1372	150.92	0.00173781	-0.026812	0.0007478	**0.0870089**	**0.00870089**	0.03533	0	**-2203**	**220**	
Ra-226 from average Pa-234 Th-234	**186.2**	5929.04	315.57	-2453.411843	-0.00562059	1372	150.92	0.00173781	-0.007358	0.0007478	**0.0870089**	**0.00870089**	0.03533	0	**-604**	**60**	
Pb-214	**352**	16970.07	493.96		0.03887724	2940	163	0.00372387	0.0351534	0.0011503	**0.0362999**	**0.00362999**	0.3534	0	**692**	**69**	**0.15**
Bi-214	**609.3**	11654.36	388.76		0.02669932	2532	126	0.00320709	0.0234922	0.0009048	**0.0178704**	**0.00178704**	0.4516	0	**735**	**74**	**0.20**
Bi-214	**1764**	1803.6	150.92		0.00413192	1461	56	0.00185054	0.0022814	0.0003529	**0.0056255**	**0.00056255**	0.1531	0	**669**	**67**	**1.20**
U-235	**144**	0	0	0	0	53	53	6.7131E-05	-6.71E-05	6.713E-05	**0.115606**	**0.0115606**	0.1096	0	**-1**	**0**	**0.20**
	163.5	0	0	0	0	10	10	1.2666E-05	-1.27E-05	1.267E-05	**0.101404**	**0.0101404**	0.0508	0	**-1**	**0**	**0.50**
	186	5929.04	315.57	2537.62912	0.00581353	1372	150.92	0.00173781	0.0040757	0.0007478	**0.0870089**	**0.00870089**	0.572	0	**21**	**2**	**0.05**
Ac-228	**911**	317066.31	602.32		0.72637664	1738	100	0.00220139	0.7241753	0.0013857	**0.0113397**	**0.00113397**	0.258	0	**62507**	**6251**	**0.40**
Pb-212	**238.6**	2538689.5	1573.63		5.8159593	3661	178	0.00463711	5.8113222	0.0036121	**0.0625507**	**0.00625507**	0.436	0	**53810**	**5381**	**0.08**
Bi-212	**727.3**	110526.31	360.57	101242.1	0.23193854	392	70.56	0.00049652	0.231442	0.0008309	**0.0145585**	**0.00145585**	0.0674	0	**59562**	**5956**	**1.10**
Tl-208	**583.1**	544913.19	834.84		1.24835784	1710	112	0.00216593	1.2461919	0.0019178	**0.0188315**	**0.00188315**	0.845	19776.44015	**55026**	**1978**	**0.10**
K-40	**1461**	12646.55	196.34		0.02897236	13256	129	0.01679035	0.012182	0.0004786	**0.006865**	**0.0006865**	0.1066	0	**4204**	**420**	**3.50**
Cs-137	661.6	0	0		0	83	73.04	0.00010513	-0.000105	9.251E-05	**0.016218**	**0.0016218**	0.851	0	**-1.92**	**0.19**	**0.10**

***Table 1**: Radionuclides and radioactivity in the parisite crystals.*

4. CONCLUSIONS

The key conclusions drawn from the present research are the following:

Typical parisite crystals from Snowbird deposit (Montana/USA) exhibited elevated actinide content. Thorium was detected in exceptionally high concentration by point SEM-EDS analyses, whereas U was measured (64 ppm) in bulk by ICP-MS after acid-dissolution. Minor μm-sized inclusions, investigated by Laser micro-Raman correspond to goethite, thus not contributing to the actinide content. Further γ-ray Spectroscopy measurements confirmed the presence of U and Th and showed enhanced radioactivity due to Th-232 (57,726 Bq/kg) and U-238 (599 Bq/kg). The results contribute to the actinide mineralogy & geochemistry in REE fluorcarbonate-minerals and make obvious the requirement for more relevant research regarding REE geological materials and deposits.

References

Anenburg, Michael, Sam Broom-Fendley, and Wei Chen. "Formation of rare earth deposits in carbonatites." Elements: An International Magazine of Mineralogy, Geochemistry, and Petrology 17.5 (2021): 327-332.

Christy, Andrew G., Igor V. Pekov, and Sergey V. Krivovichev. "The Distinctive Mineralogy of Carbonatites." Elements: An International Magazine of Mineralogy, Geochemistry, and Petrology 17.5 (2021): 333-338.

Grice, Joel D., Vincent Maisonneuve, and Marc Leblanc. "Natural and synthetic fluoride carbonates." Chemical Reviews 107.1 (2007): 114-132.

Kogarko, L. N., et al. "Uranium and thorium in carbonatitic minerals from the Guli massif, Polar Siberia." Geochemistry International 51 (2013): 767-776.

Louvel, M., Etschmann, B., Guan, Q. et al. Carbonate complexation enhances hydrothermal transport of rare earth elements in alkaline fluids. Nat Commun 13, 1456 (2022).

Metz et al. "Geology and geochemistry of the Snowbird deposit, Mineral County, Montana." Economic Geology 80.2 (1985): 394-409.

Onuonga, Isaac Oriechi. Geochemistry and mineralization of Buru and Kuge volcanic carbonatite centres, western Kenya. PhD, University of St. Andrews (United Kingdom), 1997.

Onuonga, I. O., and P. Bowden. "Hot-spring and supergene lanthanide mineralization at the Buru carbonatite centre, Western Kenya." Mineralogical Magazine 64.4 (2000): 663-673.

Rasoamalala, V., et al. "Geology of bastnaesite and monazite deposits in the Ambatofinandrahana area, central part of Madagascar: An overview." Journal of African Earth Sciences 94 (2014): 128-140.

Samson, Iain M., Scott A. Wood, and Kevin Finucane. "Fluid inclusion characteristics and genesis of the fluorite-parisite mineralization in the Snowbird deposit, Montana." Economic Geology 99.8 (2004): 1727-1744.

Yaxley, Gregory M., Bruce A. Kjarsgaard, and A. Lynton Jaques. "Evolution of carbonatite magmas in the upper mantle and crust." Elements: An International Magazine of Mineralogy, Geochemistry, and Petrology 17.5 (2021): 315-320.